ACS APPLIED MATERIALS & INTERFACES

Research Article

www.acsami.org

Enhanced Visible-Photocatalytic Activity of Anodic TiO_2 Nanotubes Film via Decoration with $CuInSe_2$ Nanocrystals

Yulong Liao,*[,†,‡] Huaiwu Zhang,*[,†] Zhiyong Zhong,[†] Lijun Jia,[†] Feiming Bai,[†] Jie Li,[†] Peng Zhong,[§] Hua Chen,[§] and Jin Zhang[∥]

[†]State Key Laboratory of Electronic Thin Film and Integrated Devices, University of Electronic Science and Technology, Chengdu 610054, China

[‡]Electronic Materials Research Laboratory, Xi'an Jiaotong University, Xi'an 710049, Shaanxi, China

[§]School of Technical Physics, Xidian University, Xi'an 710071, China

[∥]Sun Harmonics Technology Co., LTD, Hangzhou 311121, China

Supporting Information

ABSTRACT: The fabrication and photocatalytic properties of visible-light driven $CuInSe_2/TiO_2$ heterojunction films are reported. $CuInSe_2$ nanoparticles (NCs) were synthesized using a solvothermal method and then decorated onto self-organized anodic TiO_2 nanotube (NT) arrays through an electrophoretic deposition process, forming a $CuInSe_2$ NC/TiO_2 NT hetero-structure film. An increase in deposition time produced an increased amount of $CuInSe_2$ NCs loaded onto the TiO_2 NT arrays, expanding the light-absorption range of the $CuInSe_2$ NCs/TiO_2 NTs film from 400 nm to 700 nm. Photocatalytic degradation results show that activities of the $CuInSe_2$ NCs/TiO_2 NTs films were significantly enhanced compared to that of pure TiO_2 NTs (degradation rate constant k increased from 3×10^{-3} min^{-1} to $>1 \times 10^{-2}$ min^{-1}). Particularly, the $CuInSe_2$ NCs/TiO_2 NTs with 50 min electrophoretic deposition show the highest degradation rate, $k = 1.6 \times 10^{-2}$ min^{-1} (more than 5 times greater than that of the pure TiO_2 NTs film), due to optimization of $CuInSe_2$ NCs loading and a well-maintained open TiO_2 tube-mouth configuration.

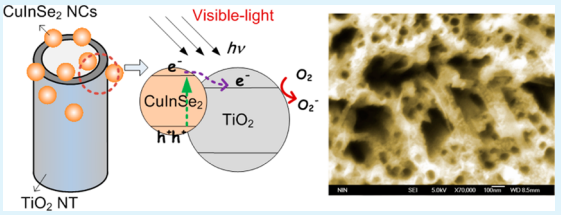

KEYWORDS: *TiO_2 nanotubes, $CuInSe_2$ nanocrystals, heterojunctions, photocatalytic activity*

1. INTRODUCTION

During the past decades, organic pollution in water has been one of the most serious environmental problems, and great efforts have been applied using various technologies to eliminate these toxic chemicals from water.[1−4] Among these strategies, semiconductor photocatalysis has been shown to be a promising remediation technology with unique advantages, such as energy efficiency and no secondary pollution.[5−7] In particular, titanium dioxide (TiO_2), a wide-band semiconductor (~3.2 eV), is particularly useful for organic degradation. When TiO_2 was properly irradiated, electron/hole pairs or excitons could be generated by incoming photons, which either migrate to the material surface or recombine and dissipate the energy as heat. Those on the surface can then participate in redox reactions and generate reactive oxygen species (ROS). Both the photo-generated electron/hole pairs and ROS contribute to the degradation and removal of organic pollutants from water.[8,9] TiO_2-based materials are still among the most widely used semiconductor photocatalysts, due to their low cost, high catalytic activity, good chemical and mechanical stability, and non-toxicity to environment and human beings.[10−14]

However, there are two major concerns during the application of TiO_2 photocatalysts: The first is how to recycle the TiO_2 photocatalysts; most photocatalyst materials are used in powder form, which is very difficult to recover for beneficial reuse. The second is how to increase the photocatalytic light absorption range. Due to its wide band-gap nature (~3.2 eV), TiO_2 is excited only by ultraviolet light.[15−18] Separating and recycling suspended TiO_2 powder photocatalysts from treated water has many difficulties and energy cost problems. Immobilized TiO_2 photocatalyst materials have been shown to be good candidates to solve this problem and have attracted increased interest. One class of outstanding photocatalyst materials are anodic TiO_2 nanotube (NT) films, not only due to their large surface area but also due to their inherent immobilization, which can reduce the energy and material cost of separating the photocatalysts.[19−23] Nevertheless, their large band-gap along with a fast recombination rate of the photogenerated electron/hole pairs still limit their photocatalytic performance and hinder commercial and industrial applications. Many efforts have been attempted to further overcome such impediments, one of which is to build heterogeneous TiO_2 photocatalysts with narrow band gaps.[24,25] For instance, TiO_2/CdS or TiO_2/CdSe heterojunction photocatalysts have been widely studied for organic pollutant decomposition under visible irradiation.[26−30] Here,

Received: August 6, 2013
Accepted: October 8, 2013
Published: October 8, 2013

CdS or CdSe, having a narrow band gap, not only acts as a visible-light sensitizer but also enhances the electron/hole pair separation in the heterojunction system at the same time. However, considering environmental regulations, the intrinsic toxicity of Cd casts doubts on the future applicability of the Cd compounds, despite their great electrical and optical properties. In light of this, Cd-free alternative materials were proposed, such as I-III-VI_2 nanocrystals with fewer environmental impacts than Cd,[31−33] although so far synthesis of I-III-VI_2 nanocrystals is much less developed.

Herein, we report a new study on the fabrication and photocatalytic performance of a visible-light heterojunction photocatalyst, which consists of $CuInSe_2$ nanocrystal (NCs)/TiO_2 NT arrays as shown in Figure 1a. $CuInSe_2$, a direct energy gap material (~1.04 eV), belongs to one of the I-III-VI_2 ternary compounds, has a large absorption coefficient, and is composed of much less toxic elements.[33,34] Meanwhile, the optical absorption of the $CuInSe_2$ NCs lies within the visible-light range and therefore matches well to the solar spectrum. In this study, the $CuInSe_2$ NCs with uniform size distribution were synthesized using solvothermal methods and decorated onto highly ordered anodic TiO_2 NT arrays by using electrophoretic deposition (EPD) and subsequently used as a visible-light sensitizer. The as-obtained films have a two-component structure as $CuInSe_2$ NCs/TiO_2 NTs, with various $CuInSe_2$ loading ratio. The $CuInSe_2$ NCs/TiO_2 NT films were characterized by scanning electron microscopy, X-ray diffraction, UV−vis absorption spectroscopy, etc. Photocatalytic activities of the $CuInSe_2$ NCs/TiO_2 NT heterojunction films were investigated by evaluating the photocatalytic degradation of methyl orange aqueous solution at room temperature.

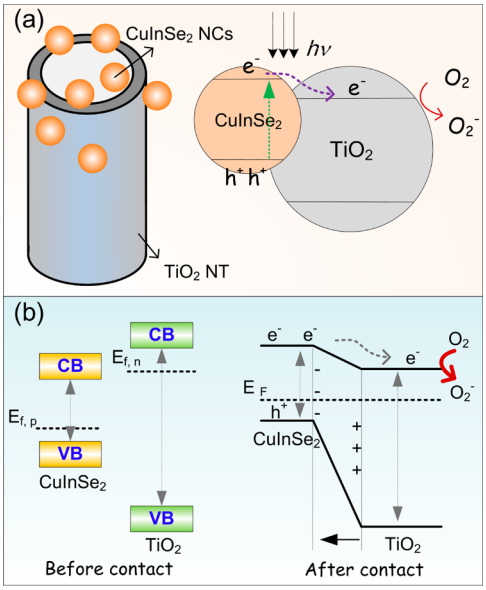

Figure 1. (a) Schematic diagram of $CuInSe_2$ NC/TiO_2 NT arrays heterojunction system. (b) Diagram of the band energy of $CuInSe_2$ and TiO_2 before and after contact, along with electron-hole pair separation and transmission $CuInSe_2$ /TiO_2 heterojunction system.

2. EXPERIMENTAL SECTION

All chemicals used in our experiment were received from commercial companies and used without further purification (analytical- grade reagents). Deionized water with a resistance of 18.3 MΩ·cm was used in the experiment.

2.1. Synthesis of TiO_2 NT Arrays. TiO_2 nanotube arrays were synthesized by an electrochemical process in a fluorine-containing nonaqueous electrolyte as described by Grimes et al.[35−37] Briefly, Ti metal sheets (>99.6%, Beijing Nonferrous Metal Research Institute) were cut into small pieces (1.5 cm × 5 cm), cleaned in sonication baths in acetone and ethanol each for 10 min, and then dried at room temperature. One piece of cleaned Ti sheet was taken as the anode with a platinum (Pt) foil as the counter electrode and directly immersed into the electrolyte (294 mL glycol, 6 mL H_2O, and 1 g NH_4F). A constant potential of 60 V was applied across the two electrodes with a distance of 2.5 cm by using a DC power supply (Model GPS-3303c, GW Instrument Co., Ltd Taiwan). The anodic oxidation was carried out in this two-electrode configuration for 3 h at 7 °C, obtaining highly ordered TiO_2 NT arrays on the Ti sheet substrate. To induce crystallinity, the highly ordered TiO_2 NT arrays were annealed at 450 °C for 2 h.

2.2. Synthesis of $CuInSe_2$ NCs. $CuInSe_2$ NCs were synthesized in a non-coordinating oleylamine solvent.[38,39] In a typical process, 1 mmol CuCl, 1 mmol $InCl_3{\cdot}4H_2O$, 2 mmol Se powder, and 10 mL oleylamine were mixed together and loaded in a three-neck flask. The system was heated to 70 °C under a nitrogen atmosphere with stirring for 90 min to remove water and oxygen. Then the mixture solution was quickly heated to 220 °C and incubated for 4 h. After that, the reaction vessel was allowed to naturally cool to room temperature. Then well-dispersed $CuInSe_2$ NC black "inks" were obtained by further purification (using ethanol and chloroform) along with centrifugation. It is should be noted that, to obtain high quality $CuInSe_2$ NCs, vigorous stirring is required through the synthesis process. The typical product yield of the well-dispersed $CuInSe_2$ NCs was around 15%.

2.3. Decoration of TiO_2 NT Arrays with $CuInSe_2$ NCs by Using an Electrophoresis Method. Electrophoresis allows for simple fabrication of large-scale and complex-shaped thin films, with a high level of coating thickness control, with simple equipment required and low cost.[40] Therefore, we used this method to decorate the TiO_2 NT arrays with the $CuInSe_2$ NCs. First, the as-prepared $CuInSe_2$ NCs were re-dispersed in chloroform with a typical concentration of 10^{-6} mol L^{-1}. Then, the highly-ordered TiO_2 NT arrays electrodes were immersed in the $CuInSe_2$ NCs solution, and a constant voltage of 150 V was applied for 25, 50, or 75 min. After the electrophoresis process, the electrodes were rinsed with chloroform several times to wash off the unbounded $CuInSe_2$ NCs. Finally, the $CuInSe_2$ NC-decorated TiO_2 NT arrays were annealed at 300 °C for 15 min to form $CuInSe_2$/TiO_2 heterojunction photocatalyst.

2.4. Characterization. X-ray diffraction (XRD) analysis was employed to characterize the crystallinity of the as-synthesized TiO_2 NT arrays and $CuInSe_2$ NCs (a D/max 2400 X Series X-ray diffractometer). The X-ray radiation source was Cu Kα, obtained at 40 kV, 100 mA, and the scanning speed was 10°/min at a step of 0.02°. Transmission electron microscopy (TEM, JEM2100, JEOL Inc., Japan) was used to characterize the structural and morphological properties of the $CuInSe_2$ NCs. A field emission scanning electron microscopy (FESEM, JSM-7000F, JEOL Inc. Japan) was employed to characterize the morphology of the $CuInSe_2$/TiO_2 films. UV−vis absorption spectra of the samples were obtained by a JASCO V-570 UV/VIS/NIR spectrometer. The specific surface area was obtained by scraping the TiO_2 NT arrays from the Ti substrate and then measuring the loose NTs by Brunauer-Emmett-Teller (BET) analysis via nitrogen adsorption at 77 K (model ASAP 2020, Micromeritics, USA).

2.5. Photocatalytic activity measurement. Photocatalytic activities of $CuInSe_2$/TiO_2 heterojunction photocatalysts were evaluated on the basis of the degradation of methyl orange (MO) as model organic pollutants in aqueous solutions (40 mL total volume, 20 mM). The $CuInSe_2$/TiO_2 NT films (3.0 × 1.5 cm^2 surface area, total mass = 0.04 g) were immersed in the solution and irradiated with six 4-W visible bulbs (Toshiba, Cool white, FL4W, Japan). Then the solution was magnetically stirred in the dark for 1 h to ensure adsorption−desorption equilibrium prior to photocatalytic degradation. Photodegradation experiments lasted 160 min with 1-mL samples removed periodically and were carried out in an open quartz

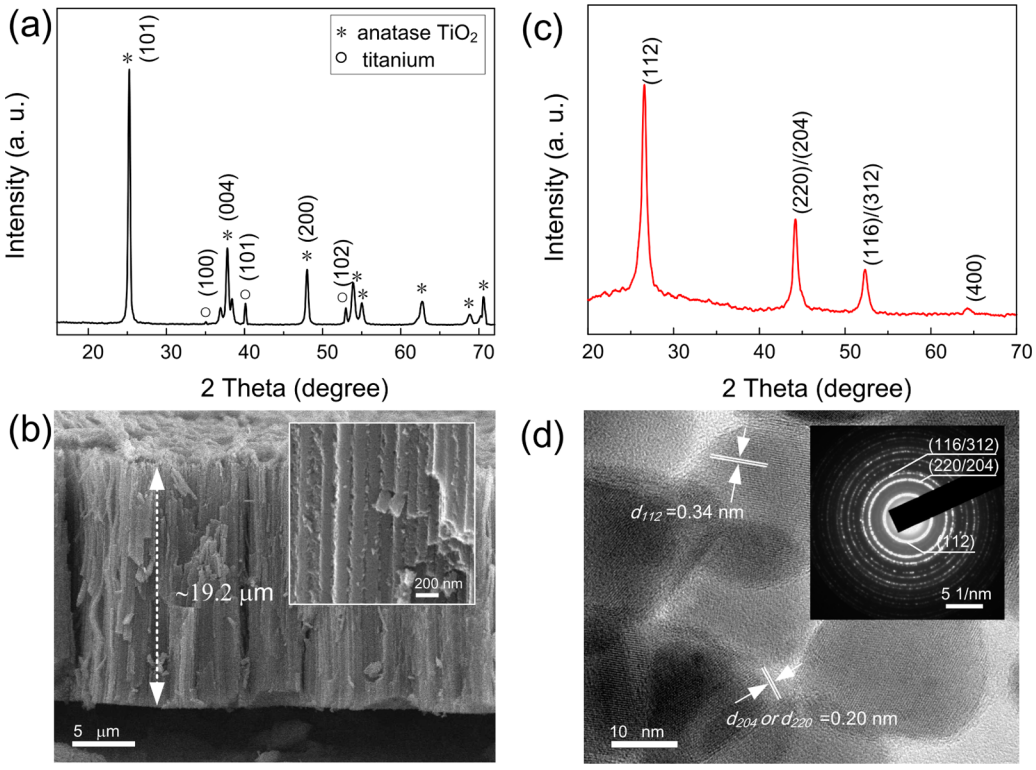

Figure 2. Anatase TiO_2 NT arrays by anodization: (a) XRD pattern and (b) SEM image. As-prepared $CuInSe_2$ NCs: (c) XRD patterns and (d) TEM image. The inset of panel d is the corresponding selected area electrical diffraction (SAED) patterns of the as-prepared $CuInSe_2$ NCs.

photoreaction vessel with rapid stirring at 23 °C. The concentration of the residual MO was measured by a UV−vis spectrometer at 463 nm on the basis of the Beer−Lambert Law. The degradation efficiency of the MO can be defined as follows:

$$C_t/C_0 = A_t/A_0 \quad (1)$$

where C_0 and C_t are the MO concentration at time zero and t (min), respectively, and A_0 and A_t are the corresponding measured absorbance at time zero and time t, respectively. The total organic carbon (TOC) during the degradation process was monitored by a Shimadzu 500 TOC analyzer.

3. RESULTS AND DISCUSSION

Anodized TiO_2 NTs are usually amorphous in structure and need be crystallized by high temperature sintering before various applications. Figure 2a shows the XRD patterns of the as-obtained TiO_2 NT arrays on the Ti sheet substrate after thermal annealing at 450 °C for 2 h. The TiO_2 NT arrays had a highly crystalline structure, judging from their sharp diffraction peaks and strong intensities. All of the diffraction peaks can be indexed to the anatase phase of TiO_2 (JCPDS No. 21-1272), except for a few characteristic peaks that belong to the titanium substrate. For instance, four peaks located at 2θ = 25.3°, 37.8°, 48.05°, and 55.06° could be attributed to the anatase (101), (004), (200), and (211) diffractions, respectively.[41] Figure 2b shows the FESEM image of the TiO_2 NT arrays. It reveals that the TiO_2 NT arrays consisted of hundreds of self-organized TiO_2 NTs that grew vertically from the Ti substrate with thickness up to ~19.2 μm. Meanwhile, it can be seen that these TiO_2 NTs were highly ordered with a diameter of ~110 nm. These results indicate that highly ordered anatase TiO_2 NT arrays were successfully fabricated by the anodization process.

Figure 2c and d shows the XRD patterns and a HRTEM image, respectively, of the as-synthesized $CuInSe_2$ NCs. XRD patterns suggest the synthesized products have a highly crystalline nature, as shown in Figure 2c. All of the characteristic diffraction peaks of $CuInSe_2$ are clearly observed, such as (112), (220)/(204), and (116)/(312) peaks at 2θ = 26.6°, 44.7°, and 52.8°, respectively. Moreover, XRD results also indicate that the as-synthesized $CuInSe_2$ NCs have a tetragonal structure, and the calculated lattice parameters are as follows: $a = b$= 0.577 nm and c = 1.162 nm, which are in line with reported parameters of $a = b$ = 0.578 nm and c = 1.162 nm.[42] By the Scherrer equation, the average diameter of the $CuInSe_2$ NCs calculated from (112) diffraction peaks is about 13.5 nm. Figure 2d shows the HRTEM images of the $CuInSe_2$ NCs synthesized at 220 °C for 4 h, and the outline figure of those individual $CuInSe_2$ NCs can be easily observed. The average size of the $CuInSe_2$ NCs is about 15 nm, which is a little bigger than the calculated average size from XRD results (~13.5 nm). As shown in Figure 2d, the lattice fringe d = 0.34 nm and 0.2 nm can be assigned to the (112) and (220)/(204) lattice planes of the tetragonal $CuInSe_2$ NCs, respectively. Moreover, corresponding selected area electrical diffraction (SAED) patterns also indicate the nanocrystal structure of the as-synthesized $CuInSe_2$ NCs, as shown in the inset of Figure 2d; the three rings refer to the (112), (220)/(214), and (116)/(312) reflection direction. It can be concluded that well crystallized tetragonal $CuInSe_2$ NCs were prepared, which were later used as a narrow-band semiconductor materials to decorate the wide-band semiconductor TiO_2 NT arrays.

Figure 3 shows the top-view SEM images of the highly ordered anatase TiO_2 NT arrays before and after decoration with the as-synthesized $CuInSe_2$ NCs through an electrophoretic deposition process. Before deposition, the open tube mouth of TiO_2 NT arrays can be clearly observed and the self-organized TiO_2 NTs are highly ordered and closely packed

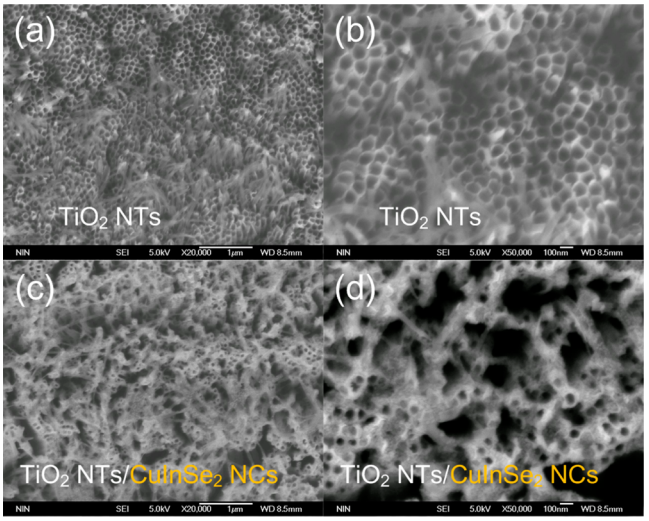

Figure 3. SEM images of the TiO_2 NT arrays (a, b) before and (c, d) after decoration with the $CuInSe_2$ NCs (electrophoretic deposition at 150 V for 25 min).

together, as shown in Figure 3a and b. The average tube diameter is about 110 nm, with an average wall thickness of 15 nm. Figure 3c and d shows the morphologies of the TiO_2 NT arrays after decoration with $CuInSe_2$ NCs. By comparing with Figure 3a and b, it can be seen that the $CuInSe_2$ NCs were effectively deposited on the top surface (partially inside) of the TiO_2 NT arrays by the electrophoresis process at 150 V for 25 min. Moreover, the tube-pore mouths are still open after the deposition, indicating that well-ordered pore structure can be maintained, which is very important for photocatalytic performance.[43] These results suggest that the as-synthesized $CuInSe_2$ NCs were successfully immobilized with TiO_2 NT arrays, the deposition process does not damage the highly ordered TiO_2 NT arrays, and the heterogeneous structure of the $CuInSe_2$ NCs/TiO_2 NTs was obtained.

To further investigate the $CuInSe_2$ NCs/TiO_2 NT heterostructured films, an elemental analysis was carried out using energy-dispersive X-ray spectroscopy (EDX). Supplementary Figure S1 shows a typical EDX spectrum of the $CuInSe_2$ NCs/TiO_2 NT film after 25 min electrophoretic deposition, and the characteristic peaks belonging to Ti, Cu, In, Se were observed, confirming the successful deposition of $CuInSe_2$ NCs. It should be noted that the EDX results show elemental composition of only the top surface of the $CuInSe_2$ NCs/TiO_2 NT array (within several micrometers at most). The content ratio of Cu, In, and Se is about 2.4 atom %, 2.7 atom %, and 7.8 atom %, respectively, as shown in Table 1. The element ratio of Cu:In:Se roughly agrees with the formula ratio 1:1:2 of $CuInSe_2$. Supplementary Figure S2 shows that different elements of the $CuInSe_2$ NCs/TiO_2 NT films vary with increased electrophoresis time. Cu, In, and Se contents increased from 2.4 to 12.0 atom %, from 2.7 to 19.9 atom %, and from 7.8 to 47.5 atom %, respectively, with electrophoresis duration increasing from 25 to 75 min. The elemental content of the $CuInSe_2$ NCs/TiO_2 NTs films were summarized as shown in Table 1, and it can be easily found that the ratio of Cu/Ti, In/Ti, and Se/Ti increased with the electrophoresis time. Meanwhile, an increase in the relative concentration of In and Se can be observed with the increase of deposition time, which may be because the $CuInSe_2$ NCs have a relatively large size distribution, so during the electrophoresis procedure smaller (more mobile) $CuInSe_2$ NCs get deposited onto the TiO_2 NTs first, followed by the bigger ones. Smaller and bigger $CuInSe_2$ NCs do not have the same composition, causing the gradual change in the total composition of the $CuInSe_2$ NCs layer. The results indicate that an increasing amount of $CuInSe_2$ NCs was successfully decorated on the surfaces of the TiO_2 NT arrays as the deposition duration increased.

UV−vis absorption spectrum can be used to investigate optical properties of the $CuInSe_2$ NCs/TiO_2 NTs films. Figure 4 shows the normalized UV−vis absorption spectra of the pure

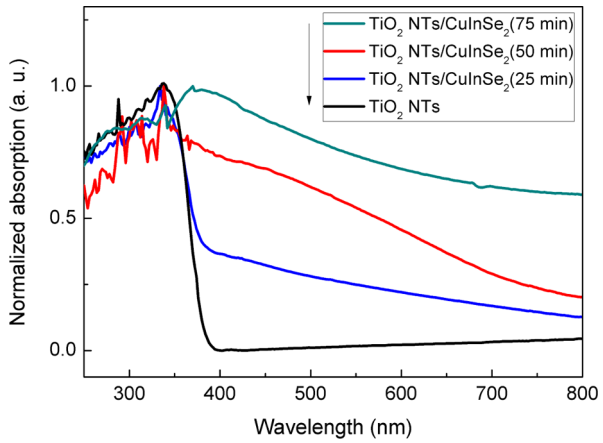

Figure 4. Normalized UV−vis absorption spectra of the $CuInSe_2$ NCs/TiO_2 NT arrays films with electrophoretic time increased from 25 min to 75 min.

TiO_2 NT film and the $CuInSe_2$ NCs/TiO_2 NTs films with different deposition duration from 25 min to 75 min. It can be seen that the absorption range of the undecorated TiO_2 NT film lies only within the ultraviolet region (<380 nm), while that of the $CuInSe_2$ NCs/TiO_2 NT films cover almost the entire visible region (about 400−700 nm). Meanwhile, an increased absorption was also observed as the $CuInSe_2$ NCs deposition duration increased.

Photocatalytic activities of the $CuInSe_2$ NCs/TiO_2 NT films were evaluated through degradation of MO aqueous solution, with degradation kinetics shown in Figure 5a. It can be seen

Table 1. Element Contents Based on EDX Results and First Order Constant *k* Values for the $CuInSe_2$ NC/TiO_2 NT Films with Various Electrophoresis Times

	EDX results, atom %					
samples	Cu (error)	In (error)	Se (error)	Ti (error)	O (error)	av *k*, min^{-1}
$CuInSe_2$ NCs/TiO_2 NTs; 75 min	12.0 (2.17)	19.9 (0.67)	47.5 (0.38)	7.79 (0.46)	12.9 (0.33)	0.006
$CuInSe_2$ NCs/TiO_2 NTs; 50 min	7.3 (2.31)	10.3 (0.67)	26.0 (0.4)	37.5 (0.46)	18.9 (0.44)	0.016
$CuInSe_2$ NCs/TiO_2 NTs; 25 min	2.4 (3.22)	2.7 (0.85)	7.8 (0.55)	46.8 (0.59)	40.3 (0.73)	0.010
TiO_2 NTs						0.003

dx.doi.org/10.1021/am403264q | ACS Appl. Mater. Interfaces 2013, 5, 11022−11028

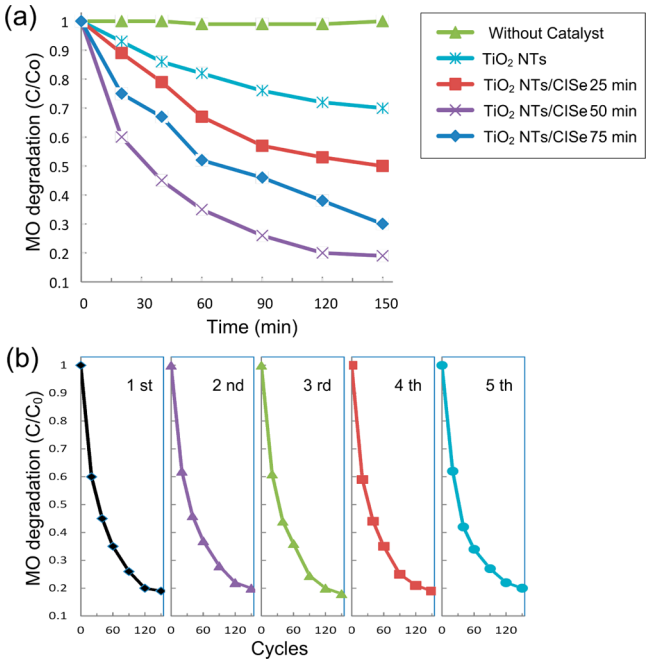

Figure 5. (a) Photocatalytic degradation kinetics of MO aqueous solution with the $CuInSe_2$ NC/TiO_2 NT arrays films as photocatalytic panel. (b) Photocatalytic cycling test using the $CuInSe_2$ NCs/TiO_2 NT arrays with 50 min electrophoretic deposition.

that, for the blank testing, negligible MO degradation was observed when no photocatalyst applied, which indicates the MO solution was stable as a probe to test the activities of the $CuInSe_2$ NCs/TiO_2 NTs films. When a photocatalyst panel was included, significant MO degradation was achieved immediately for all of the samples. Figure 5a shows that around 28% of the MO was photo-catalytically degraded by using the pure anatase TiO_2 NT array film after 150 min of irradiation, while over 50% of the MO was degraded using the $CuInSe_2$ NCs/TiO_2 NTs films, indicating an enhanced photocatalytic activity. Supplementary Figure S3 shows the curves of $-\ln(C/C_0)$ variation with degradation time, and a liner relation can be easily observed for all of the samples, which indicates that the photocatalytic degradation of the MO followed pseudo-first-order kinetics and the kinetic reaction can be expressed as follows:

$$A_t = A_0\, e^{-kt} \qquad (2)$$

where k (min^{-1}) is the degradation rate constant. The calculated first order constant k values for all of the $CuInSe_2$ NCs/TiO_2 NTs films are summarized in Table 1. It can be seen that the degradation constant k value of the pure TiO_2 NTs is only about 0.003 min^{-1}, which increased two-fold to 0.006 min^{-1} for the $CuInSe_2$ NCs/TiO_2 NTs film with 25 min deposition. When the $CuInSe_2$ NCs deposition duration increased from 25 to 50 min, the degradation rate constant k value increased from 0.006 min^{-1} to the maximum value of 0.016 min^{-1}. However, a decreased k value was observed (0.010 min^{-1}) when the $CuInSe_2$ NCs deposition duration was 75 min. Therefore, 50 min electrophoretic deposition is the optimized duration in the study. The relationship between the degradation rate constant k values and the $CuInSe_2$ NCs electrophoretic deposition time is shown in Supplementary Figure S4. Although the TOC testing showed a hysteretic degradation kinetic (see Supplementary Figure S5), the MO solution was found evidently decompounded by the $CuInSe_2$ NCs/TiO_2 NTs films. On the basis of the above results, it can be concluded that the photocatalytic performance of the TiO_2 NT array film can be greatly enhanced by introducing the $CuInSe_2$ NCs. The enhanced photocatalytic activity is mainly ascribed to two aspects:[44,45]

(a) The $CuInSe_2$ NCs improve the absorption efficiency of the $CuInSe_2$ NCs/TiO_2 NT array films almost through the entire visible-light region, as shown in Figure 4. This allows more photons to be absorbed and generates more active electron-hole pairs, which subsequently contributes to the photocatalytic enhancement;

(b) The formation of the $CuInSe_2$ NCs/TiO_2 NT heterojunctions can suppress the recombination of the photogenerated electron-hole pairs and prolong the charge-carrier's lifetime, which also benefited the $CuInSe_2$ NCs/TiO_2 NT film's photocatalytic performance. The band gap structures and their Fermi energy levels are schematically shown in Figure 1b.

Moreover, BET analysis indicates the $CuInSe_2$ NCs/TiO_2 NTs-50 min sample has a specific area of ~39 m^2/g, and cycling test results indicate that the as-obtained $CuInSe_2$ NCs/TiO_2 NTs heterojunction films are very stable and have a repeatable performance. Figure 5b shows that the $CuInSe_2$ NCs/TiO_2 NTs-50 min sample kept its high activity after 5 cycles. This result indicates the $CuInSe_2$ NCs were firmly attached to the TiO_2 NT arrays and thus successfully immobilized.

To better understand the influence of $CuInSe_2$ NCs on photocatalytic activities of the $CuInSe_2$ NCs/TiO_2 NT heterojunction films, we propose a possible deposition mechanism of the $CuInSe_2$ NCs on the TiO_2 NT array films with the electrophoresis time as illustrated in Figure 6. It can be

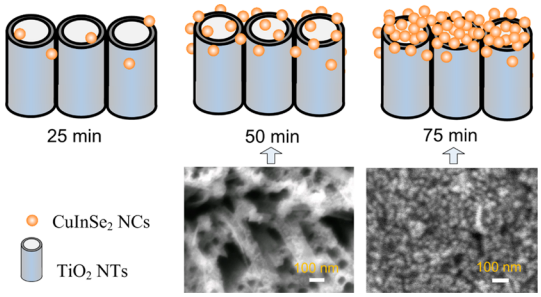

Figure 6. Schematic of the deposition process of the $CuInSe_2$ NCs on the TiO_2 NTs array films with the electrophoresis time, the insets are the corresponding SEM images.

observed from Figure 6 that, at 25 min, scattered $CuInSe_2$ nanocrystal particles were deposited on the TiO_2 NTs forming a $CuInSe_2$ NCs/TiO_2 NTs heterojunction structure. The $CuInSe_2$ NCs could be activated by visible-light photons, and the photogenerated electrons would migrate to the TiO_2 NTs enabling the visible-light photocatalytic activity with an overall enhancement as we observed in Figure 5. By increasing the electrophoresis time to 50 min, more $CuInSe_2$ NCs were decorated onto the TiO_2 NTs and acted as a visible-light sensitizer for photocatalytic reaction, without blocking the open tube mouth of the TiO_2 NTs at the same time. The $CuInSe_2$ NCs/TiO_2 NTs-50 min sample shows the highest degradation rate (k = 0.016 min^{-1}), which was almost 5 times higher than that of the pure TiO_2 NT arrays (k = 0.003 min^{-1}), as shown in Table 1 and Supplementary Figure S4. At 75 min deposition

time, however, excessive $CuInSe_2$ NCs were deposited on the TiO_2 NTs. The inset SEM of Figure 6 shows that the $CuInSe_2$ NCs started forming a film-like layer and blocked most of the open tube mouths of the TiO_2 NT arrays. With fewer open tube mouths, the molecular transportations channels are reduced: both MO molecules and photo-generated ROS diffusion will be restricted out of and into solution, leading to the decrease in degradation rate, k, back to 0.010 min^{-1}. Therefore, there should be a balance between $CuInSe_2$ NCs loading mass and retaining the open tube-mouth configuration for achieving the best photocatalytic activity of the $CuInSe_2$ NCs/TiO_2 NTs heterojunction films. Since the above assumption is consistent with SEM, EDX, and photocatalytic degradation results, we believe that the $CuInSe_2$ NCs with a proper electrophoretic deposition quantity play a significant role in the enhanced visible-light photocatalytic activities of the $CuInSe_2$ NCs/TiO_2 NT heterojunction films.

4. CONCLUSIONS

Highly-ordered TiO_2 NT arrays and well-dispersed tetragonal $CuInSe_2$ NCs were successfully prepared by using a facile anodization method and a solvothermal method, respectively. The highly ordered TiO_2 NT arrays with open tube mouths were decorated with the $CuInSe_2$ NCs through an electrophoretic process, forming a $CuInSe_2$ NCs/TiO_2 NTs heterojunction film. Compared with pure TiO_2 NTs, the as-obtained $CuInSe_2$ NCs/TiO_2 NT films show enhanced photocatalytic activity towards degrading MO. The enhanced photocatalytic activities were attributed to the formation of $CuInSe_2$/TiO_2 heterojunctions, which improve the visible-light absorption efficiency and inhibit the recombination of the photogenerated electron-hole pairs. SEM, EDX, and UV–vis results indicate that increased $CuInSe_2$ NCs were immobilized on the TiO_2 NTs films with increasing electrophoresis time. The optimized electrophoretic time is 50 min in this study, and the photocatalytic activity of the $CuInSe_2$ NCs/TiO_2 NT film was enhanced more than 5 times compared to that of undecorated TiO_2 NT films, due to a proper $CuInSe_2$ NCs loading and the well-maintained open tube-mouth configuration. These results are expected to be helpful for further understanding of the preparation and photocatalytic properties of $CuInSe_2$ nanocrystal decorated TiO_2 nanotube arrays film photocatalysts.

■ ASSOCIATED CONTENT

Supporting Information

EDX spectrum in detail and additional photocatalytic results and analysis. This material is available free of charge via the Internet at http://pubs.acs.org.

■ AUTHOR INFORMATION

Corresponding Authors

*E-mail: yulong.liao@uestc.edu.cn.
*E-mail: hwzhang@uestc.edu.cn.

Notes

The authors declare no competing financial interest.

■ ACKNOWLEDGMENTS

We thank Dr. Jonathon Brame from Rice University for assistance with the language editing. This work was financially supported by the National Basic Research Program of China under Grant No. 2012CB933104 and the National Nature Science Foundation of China under Grant No. 61021061, and No. 61271037.

■ REFERENCES

(1) Qu, X.; Brame, J.; Li, Q.; Alvarez, P. J. J. *Acc. Chem. Res.* **2012**, *46*, 834–843.
(2) Lim, Y. W. L.; Tang, Y.; Cheng, Y. H.; Chen, Z. *Nanoscale* **2010**, *2*, 2751–2757.
(3) Choudhury, B.; Borah, B.; Choudhury, A. *Photochem. Photobiol.* **2012**, *88*, 257–264.
(4) Dholam, R.; Patel, N.; Adami, M.; Miotello, A. *Int. J. Hydrogen Energy* **2009**, *34*, 5337–5346.
(5) Brame, J. A.; Hong, S. W.; Lee, J.; Lee, S.-H.; Alvarez, P. J. J. *Chemosphere* **2013**, *90*, 2315–2319.
(6) Jiang, Z.; Tang, Y.; Tay, Q.; Zhang, Y.; Malyi, O. I.; Wang, D.; Deng, J.; Lai, Y.; Zhou, H.; Chen, X.; Dong, Z.; Chen, Z. *Adv. Energy Mater.* **2013**, *3*, 1368–1380.
(7) Fischer, B. B.; Krieger-Liszkay, A.; Eggen, R. I. L. *Environ. Sci. Technol.* **2004**, *38*, 6307–6313.
(8) Khan, M. A.; Akhtar, M. S.; Woo, S. I.; Yang, O. B. *Catal. Commun.* **2008**, *10*, 1–5.
(9) Macak, J. M.; Zlamal, M.; Krysa, J.; Schmuki, P. *Small* **2007**, *3*, 300–304.
(10) Choudhury, B.; Choudhury, A. *Curr. Appl. Phys.* **2013**, *13*, 1025–1031.
(11) Foong, T. R. B.; Chan, K. L.; Hu, X. *Nanoscale* **2012**, *4*, 478–485.
(12) Foong, T. R. B.; Shen, Y.; Hu, X.; Sellinger, A. *Adv. Funct. Mater.* **2010**, *20*, 1390–1396.
(13) Jha, P. K.; Gupta, S. K.; Lukačević, I. *Solid State Sci.* **2013**, *22*, 8–15.
(14) Mankad, V.; Gupta, S. K.; Jha, P. K. *Phys. E* **2011**, *44*, 614–617.
(15) Mishra, S.; Jha, P.; Pratap, A. *J. Therm. Anal. Calorim.* **2012**, *107*, 65–68.
(16) Wang, P.; Tang, Y.; Dong, Z.; Chen, Z.; Lim, T.-T. *J. Mater. Chem. A* **2013**, *1*, 4718–4727.
(17) Wang, S.; Qian, H.; Hu, Y.; Dai, W.; Zhong, Y.; Chen, J.; Hu, X. *Dalton Trans.* **2013**, *42*, 1122–1128.
(18) Xiu, Z.-m.; Zhang, Q.-b.; Puppala, H. L.; Colvin, V. L.; Alvarez, P. J. J. *Nano Lett.* **2012**, *12*, 4271–4275.
(19) Mohapatra, S. K.; Misra, M.; Mahajan, V. K.; Raja, K. S. *J. Phys. Chem. C* **2007**, *111*, 8677–8685.
(20) Park, J. H.; Kim, S.; Bard, A. J. *Nano Lett.* **2006**, *6*, 24–28.
(21) Woan, K.; Pyrgiotakis, G.; Sigmund, W. *Adv. Mater.* **2009**, *21*, 2233–2239.
(22) Zheng, Q.; Zhou, B.; Bai, J.; Li, L.; Jin, Z.; Zhang, J.; Li, J.; Liu, Y.; Cai, W.; Zhu, X. *Adv. Mater.* **2008**, *20*, 1044–1049.
(23) Liao, Y.; Brame, J.; Que, W.; Xiu, Z.; Xie, H.; Li, Q.; Fabian, M.; Alvarez, P. J. *J. Hazard. Mater.* **2013**, *260*, 434–441.
(24) Li, L.; Liu, X.; Zhang, Y.; Nuhfer, N. T.; Barmak, K.; Salvador, P. A.; Rohrer, G. S. *ACS Appl. Mater. Interfaces* **2013**, *5*, 5064–5071.
(25) Li, L.; Liu, X.; Zhang, Y.; Salvador, P. A.; Rohrer, G. S. *Int. J. Hydrogen Energy* **2013**, *38*, 6948–6959.
(26) Daskalaki, V. M.; Antoniadou, M.; Li Puma, G.; Kondarides, D. I.; Lianos, P. *Environ. Sci. Technol.* **2010**, *44*, 7200–7205.
(27) Qian, S.; Wang, C.; Liu, W.; Zhu, Y.; Yao, W.; Lu, X. *J. Mater. Chem.* **2011**, *21*, 4945–4952.
(28) Meng, Z.-D.; Zhu, L.; Ye, S.; Sun, Q.; Ullah, K.; Cho, K.-Y.; Oh, W.-C. *Nanoscale Res. Lett.* **2013**, *8*, 1–10.
(29) Lo, S.-C.; Lin, C.-F.; Wu, C.-H.; Hsieh, P.-H. *J. Hazard. Mater.* **2004**, *114*, 183–190.
(30) Li, G.; Wu, L.; Li, F.; Xu, P.; Zhang, D.; Li, H. *Nanoscale* **2013**, *5*, 2118–2125.
(31) Zhang, K.; Guo, L. *Catal. Sci. Technol.* **2013**, *3*, 1672–1690.
(32) Koo, B.; Patel, R. N.; Korgel, B. A. *J. Am. Chem. Soc.* **2009**, *131*, 3134–3135.
(33) Panthani, M. G.; Akhavan, V.; Goodfellow, B.; Schmidtke, J. P.; Dunn, L.; Dodabalapur, A.; Barbara, P. F.; Korgel, B. A. *J. Am. Chem. Soc.* **2008**, *130*, 16770–16777.

(34) Aldakov, D.; Lefrancois, A.; Reiss, P. *J. Mater. Chem. C* **2013**, *1*, 3756−3776.
(35) Grimes, C. A. *J. Mater. Chem.* **2007**, *17*, 1451−1457.
(36) Mor, G. K.; Kim, S.; Paulose, M.; Varghese, O. K.; Shankar, K.; Basham, J.; Grimes, C. A. *Nano Lett.* **2009**, *9*, 4250−4257.
(37) Prakasam, H. E.; Shankar, K.; Paulose, M.; Varghese, O. K.; Grimes, C. A. *J. Phys. Chem. C* **2007**, *111*, 7235−7241.
(38) Zhang, J.; Que, W.; Shen, F.; Liao, Y. *Sol. Energy Mater. Sol. Cells* **2012**, *103*, 30−34.
(39) Shen, F.; Que, W.; Liao, Y.; Yin, X. *Ind. Eng. Chem. Res.* **2011**, *50*, 9131−9137.
(40) Miyasaka, T.; Kijitori, Y. *J. Electrochem. Soc.* **2004**, *151*, 1767−1773.
(41) Allam, Nageh K.; G., C. A. *J. Phys. Chem. C Lett.* **2009**, *113*, 7996−7999.
(42) Guo, Q.; Kim, S. J.; Kar, M.; Shafarman, W. N.; Birkmire, R. W.; Stach, E. A.; Agrawal, R.; Hillhouse, H. W. *Nano Lett.* **2008**, *8*, 2982−2987.
(43) Mazzarolo, A.; Lee, K.; Vicenzo, A.; Schmuki, P. *Electrochem. Commun.* **2012**, *22*, 162−165.
(44) Shen, F.; Que, W.; He, Y.; Yuan, Y.; Yin, X.; Wang, G. *ACS Appl. Mater. Interfaces* **2012**, *4*, 4087−4092.
(45) He, Z.; Que, W.; Chen, J.; Yin, X.; He, Y.; Ren, J. *ACS Appl. Mater. Interfaces* **2012**, *4*, 6816−6826.